Available online at www.sciencedirect.com
ScienceDirect
Geochimica et Cosmochimica Acta 75 (2011) 4699–4712
Geochimica et Cosmochimica Acta
www.elsevier.com/locate/gca

Molecular-level modes of As binding to Fe(III) (oxyhydr)oxides precipitated by the anaerobic nitrate-reducing Fe(II)-oxidizing *Acidovorax* sp. strain BoFeN1

Claudia Hohmann [a], Guillaume Morin [b], Georges Ona-Nguema [b], Jean-Michel Guigner [b], Gordon E. Brown Jr. [c,d], Andreas Kappler [a,*]

[a] *Geomicrobiology, Center for Applied Geosciences, University of Tübingen, Germany*
[b] *Institut de Minéralogie et de Physique des Milieux Condensés, UMR 7590, CNRS, Universités Paris 6 et Paris 7 et IPGP, 140 rue de Lourmel, 75 015 Paris, France*
[c] *Surface & Aqueous Geochemistry Group, Department of Geological and Environmental Sciences, Stanford University, Stanford, CA 94305-2115, USA*
[d] *Stanford Synchrotron Radiation Lightsource, SLAC National Accelerator Laboratory, 2575 Sand Hill Road, MS 69, Menlo Park, CA 94025, USA*

Received 13 July 2010; accepted in revised form 31 January 2011; available online 23 June 2011

Abstract

Sorption of contaminants such as arsenic (As) to natural Fe(III) (oxyhydr)oxides is very common and has been demonstrated to occur during abiotic and biotic Fe(II) oxidation. The molecular mechanism of adsorption- and co-precipitation of As has been studied extensively for synthetic Fe(III) (oxyhydr)oxide minerals but is less documented for biogenic ones. In the present study, we used Fe and As K-edge X-ray Absorption Near Edge Structure (XANES), extended X-ray Absorption Fine Structure (EXAFS) spectroscopy, Mössbauer spectroscopy, XRD, and TEM in order to investigate the interactions of As(V) and As(III) with biogenic Fe(III) (oxyhydr)oxide minerals formed by the nitrate-reducing Fe(II)-oxidizing bacterium *Acidovorax* sp. strain BoFeN1. The present results show the As immobilization potential of strain BoFeN1 as well as the influence of As(III) and As(V) on biogenic Fe(III) (oxyhydr)oxide formation. In the absence of As, and at low As loading (As:Fe $\leqslant$ 0.008 mol/mol), goethite (Gt) formed exclusively. In contrast, at higher As/Fe ratios (As:Fe = 0.020–0.067), a ferrihydrite (Fh) phase also formed, and its relative amount systematically increased with increasing As:Fe ratio, this effect being stronger for As(V) than for As(III). Therefore, we conclude that the presence of As influences the type of biogenic Fe(III) (oxyhydr)oxide minerals formed during microbial Fe(II) oxidation. Arsenic-K-edge EXAFS analysis of biogenic As–Fe–mineral co-precipitates indicates that both As(V) and As(III) form inner-sphere surface complexes at the surface of the biogenic Fe(III) (oxyhydr)oxides. Differences observed between As-surface complexes in BoFeN1-produced Fe(III) (oxyhydr)oxide samples and in abiotic model compounds suggest that associated organic exopolymers in our biogenic samples may compete with As oxoanions for sorption on Fe(III) (oxyhydr)oxides surfaces. In addition HRTEM–EDXS analysis suggests that As(V) preferentially binds to poorly crystalline phases, such as ferrihydrite, while As(III) did not show any preferential association regarding Fh or Gt.

1. INTRODUCTION

The metalloid As is a class 1 non-threshold carcinogen for humans (WHO, 2004) affecting about 1-2% of the world's population via contaminated groundwater aquifers

* Corresponding author. Address: Geomicrobiology, Center for Applied Geosciences, University of Tübingen, Sigwartstrasse 10, D-72076 Tübingen, Germany. Tel.: +49 7071 2974992; fax: +49 7071 295059.
E-mail address: andreas.kappler@uni-tuebingen.de (A. Kappler).

0016-7037/$ - see front matter © 2011 Elsevier Ltd. All rights reserved.
doi:10.1016/j.gca.2011.02.044

and soils. Arsenic is mainly of geogenic origin (Smedley and Kinniburgh, 2002) and, in many cases, it is associated with Fe(III)-bearing minerals. The most environmentally relevant inorganic species of As are $As(III)O_3^{3-}$ (arsenite) and $As(V)O_4^{3-}$ (arsenate). Arsenite is the more toxic species and at neutral pH it is more mobile than arsenate. Arsenate oxoanions (e.g., $H_2AsO_4^-$ and $HAsO_4^{2-}$) and arsenite species (e.g., H_3AsO_3) sorb to the surfaces of Fe(III) (oxyhydr)oxide minerals over a wide pH range (Dixit and Hering, 2003), because they form strong inner-sphere surface complexes (Waychunas et al., 1993; Manning et al., 1998; Manning, 2002; Ona-Nguema et al., 2005), as well as hydrogen-bonded surface complexes recently proposed in the case of arsenate ions (Catalano et al., 2008).

Microaerophilic as well as facultative aerobic and anaerobic Fe(II)-oxidizing bacteria, e.g., nitrate-reducing Fe(II)-oxidizers, have the potential to co-precipitate or sorb As during Fe(II) oxidation at neutral pH that is usually followed by Fe(III)-containing mineral precipitation (Hohmann et al., 2010). An *Acidovorax* sp. strain closely related to the nitrate-reducing Fe(II)-oxidizing strain BoFeN1 that was used in the study by Hohmann et al. (2010) was recently identified in an As-contaminated Bangladesh aquifer (Sutton et al., 2009). In contrast to Fe(II)-oxidizers, Fe(III)-reducing bacteria harvest energy by coupling the oxidation of organic or inorganic electron donors to the reduction of Fe(III). This process can lead to dissolution of Fe(III)-containing minerals and thus to a release of As into the environment (Tufano and Fendorf, 2008), although binding of As to secondary Fe-bearing minerals can delay mobilization of As in Fe-rich systems (Root et al., 2007; Tufano and Fendorf, 2008; Ona-Nguema et al., 2009).

Abiotic Fe(II) oxidation leads in many cases to precipitation of amorphous or poorly crystalline Fe(III)-bearing phases (Cornell and Schwertmann, 2003), whereas biomineral formation by Fe(II)-oxidizing bacteria has been shown to produce not only poorly crystalline ferrihydrite-type solids, but also crystalline phases such as goethite, lepidocrocite, hematite, magnetite and green rusts (Chaudhuri et al., 2001; Kappler and Newman, 2004; Kappler and Straub, 2005; Kappler et al., 2005). As shown by Larese-Casanova et al. (2010) for the nitrate-reducing Fe(II)-oxidizing *Acidovorax* strain BoFeN1, the type of the biogenic Fe-bearing phases formed is strongly influenced by the geochemical conditions present during Fe(II) oxidation. The identity and crystal structure of arsenic-bearing minerals and the binding modes of As to the minerals determine the stability of the As–Fe oxide composite; therefore it is crucial to quantify the influence of As on the Fe (oxyhydr)oxide biomineral structure as well as the binding mode of As on biogenic minerals in order to predict the effectiveness of As immobilization and the stability of the As–Fe–mineral co-precipitates in the environment. Exopolymeric substances (EPS) formed by bacteria (e.g., the nitrate-dependent Fe(II)-oxidizing strain BoFeN1 (Miot et al., 2009)) could also alter the relative proportion of As surface complexes, especially in the case of arsenate whose binding mode to ferrihydrite has been shown to be influenced by carboxylates (Mikutta et al., 2010).

Immobilization of As on Fe (oxyhydr)oxides via adsorption, co-precipitation and/or surface precipitation is often used in remediation of contaminated groundwater (Buswell, 1943; Zouboulis and Katsoyiannis, 2005) as well as in commercially available filtration systems (e.g., GEH® Wasserchemie). The bonding modes of As are well characterized for abiotically formed Fe(III) (oxyhydr)oxide phases, e.g., ferrihydrite, goethite, hematite and maghemite (e.g., Waychunas et al., 1993; Manning et al., 1998; Manning, 2002; Ona-Nguema et al., 2005; Auffan et al., 2008; Morin et al., 2008). However, the binding modes of arsenite and arsenate on biogenic Fe(III) (oxyhydr)oxide phases and potential differences in binding models relative to abiotic phases is still poorly documented, except for acid mine drainage systems (Morin and Calas, 2006; Benzerara et al., 2008; Egal et al., 2009).

Based on these knowledge gaps, the objectives of this study are to (i) determine how the presence of arsenite and arsenate affects Fe(II) oxidation of the nitrate-reducing Fe(II)-oxidizing *Acidovorax* strain BoFeN1, (ii) identify the Fe(III)-bearing solids formed by BoFeN1 in the absence and presence of As(III) and As(V), and (iii) determine the binding modes, e.g., adsorption vs. co-precipitation of arsenite and arsenate by the Fe(III) (oxyhydr)oxide phases formed by BoFeN1.

2. MATERIALS AND METHODS

2.1. Microbial growth media and growth experiments

We used the chemoorganotrophic, nitrate-reducing β-Proteobacterium strain BoFeN1 that is closely related to *Acidovorax* sp. and grows mixotrophically oxidizing ferrous iron and acetate as the organic co-substrate (Kappler et al., 2005; Muehe et al., 2009). For routine cultivation of strain BoFeN1, 10 mM Na-nitrate and 5 mM Na-acetate were added to freshwater mineral medium with a reduced phosphate concentration of 1 mM as described previously (Hegler et al., 2008; Hohmann et al., 2010). For these experiments, 10–15 mM Fe(II) from a sterile 1 M $FeCl_2$ stock solution were added. This was followed by the precipitation of whitish Fe(II) carbonate and Fe(II) phosphate minerals. In order to exclude those abiotically formed minerals, the medium was filtered following established protocols (Kappler and Newman, 2004), which resulted in a solution containing 6–12 mM dissolved Fe(II). Using this medium, which was still oversaturated with respect to Fe(II)-carbonate, exclusively allows identification of the biotically precipitated Fe(III)-bearing phases. For cell viability, growth data and total (extractable) Fe(II) during Fe(II) oxidation of BoFeN1, the reader is referred to our previous publications (Kappler et al., 2005; Muehe et al., 2009).

The filtered medium was prepared and poured into sterile Schott bottles (500 mL bottles, 250 mL medium). As(III) and As(V) stock solutions (20 mM) were prepared using disodium-hydrogen arsenate heptahydrate and sodium-(meta)arsenite salt and were subsequently sterile-filtered (0.22 μm, MCE, Fisher Scientific). Appropriate volumes of these As(III) and As(V) stock solutions were added to

the bottles yielding final concentrations of 50, 200, and 500 μM. After addition of the As(V) solution, a whitish precipitate formed, which remained stable in abiotic set-ups and contains most of the added As(V). In biogenic set-ups, however, the precipitate was dissolved and the Fe(II) was oxidized by the added bacteria (BoFeN1). Five percent of a culture of strain BoFeN1 grown with acetate/nitrate (without Fe(II)) was used as the inoculum. The bottles were incubated at 28 °C in the dark until complete oxidation of Fe(II) (~8 days).

2.2. Chemical analyses

Dissolved Fe concentration was quantified to follow Fe(II) oxidation by strain BoFeN1 in the absence and presence of As. For analysis of dissolved Fe, 100 μL culture suspension were centrifuged (12,000 rpm = 9660*g*, 2 min) under anoxic conditions and analyzed for dissolved Fe(II) and Fe_{tot} with the ferrozine assay (Stookey, 1970). Dissolved As was determined for quantification of As immobilization by biogenic Fe(II) oxidation. For analysis of dissolved As, either 1.5 mL culture suspension were centrifuged (12,000 rpm = 9660*g*, 2 min), filled up to 15 mL with anoxic H_2O, filtered using an anion exchange cartridge (Meng et al., 2001) and acidified with 1% concentrated HNO3 (65%) or 5 mL of culture suspension were filtered (0.22 μm, cellulose-acetate, Fisher Scientific) and acidified with 5 mL 20 mM phosphoric acid to preserve the As redox state. Total As was quantified by inductively-coupled-plasma mass-spectrometry (ICP-MS) (ELAN 6000, Perkin-Elmer). Arsenic speciation analysis carried out in an independent experiment with an Fe-free growth medium (nitrate and acetate only) showed up to 14% As(V) after acetate oxidation and growth of strain BoFeN1 in the presence of As(III). Growth in the presence of As(V) did not influence As speciation (data not shown).

2.3. Mineralogical and spectroscopic analyses

Identification of the biogenic minerals formed in the absence and presence of As was accomplished using Mössbauer spectroscopy, XRD and X-ray absorption spectroscopy analyses (XAS) at the Fe K-edge. To improve the quality of the Mössbauer spectra, the mineral medium was spiked with ^{57}Fe (50 μL of a 1 mM ^{57}Fe stock solution (Williams and Scherer, 2004)). For Mössbauer spectroscopy analysis, 15 mL of a 4-week old culture suspension were filtered through a cellulose acetate membrane filter (0.45 μM, diameter: 13 mm; Millipore) (Fe(II) oxidation was complete after ~8 days). The wet filters were sealed between two layers of Kapton® tape under anoxic conditions. These samples were then mounted on a closed-cycle exchange-gas cryostat (Janis, USA) that allowed cooling of the sample to 4.5 K. Mössbauer spectra were collected with a constant acceleration drive system in transmission mode and with a ^{57}Co source. Spectra were calibrated against a spectrum of alpha-Fe metal foil collected at room temperature. Spectral calibration and fitting was performed with Recoil software (University of Ottawa, Canada) using Voigt-based spectral line shapes.

For XRD and XAS analyses, solid samples were harvested after 8 days by filtration (using a Steritop-GP 0.22 μm, PES, MILLIPORE filter) after complete oxidation of Fe(II) and dried at room temperature under anoxic conditions. Particular care was taken to preserve anoxic conditions during XRD and XAS analysis, e.g., sample preparation under anoxic conditions (Morin et al., 2009; Ona-Nguema et al., 2009). XRD measurements were performed on a Panalytical X'Pert Pro MPD diffractometer in Debye–Scherrer configuration with Co$K\alpha_{1,2}$ radiation (λ = 0.179 nm) on powder samples mounted in Lindeman glass tubes under an anoxic atmosphere. XRD patterns were analyzed with the Rietveld method using the XND code (Berar, 1990). Mean Coherent Domain size and strain measurements were performed using classical procedures detailed in Wang et al. (2008).

For high-resolution transmission electron microscopy (HRTEM) analysis, 1 mg of dry powder sample was suspended in 1 mL ethanol and sonicated for 10 min. About 1 μL of suspension was deposited onto a carbon-coated TEM grid using syringe and needle. The grids were then vacuum-dried within the glove box, causing evaporation of the ethanol from the suspension. Dry grids were mounted on the microscope sample holder within the glove box and were then rapidly transferred within an anoxic container to the microscope vacuum chamber. HRTEM images and Energy Dispersive X-ray Spectroscopy (EDXS) data spectra were taken using a JEOL™ 2100F TEM instrument. HRTEM data were processed using the ImageJ 1.34r program package.

X-ray Absorption Fine Structure (EXAFS) and X-ray Absorption Near-edge Structure (XANES) spectra were collected at 10 K at the SSRL 11-2 wiggler beamline (As K-edge), and at the SOLEIL Samba bending magnet beamline (Fe K-edge). For As K-edge measurements, particular care was taken to limit beam damage to the sample by moving the focused beam (0.5×1 mm^2) about 1 mm between each EXAFS scan (Wang et al., 2008). EXAFS data were extracted following classical procedures reported in previous studies (Morin et al., 2009; Ona-Nguema et al., 2009). Fe K-edge XANES and EXAFS spectra of BoFeN1 samples were analyzed by linear combination least squares fitting (LCF) of experimental data using XANES and EXAFS spectra of model compounds selected from a large database of model Fe (oxyhydr)oxide compounds (see the model compounds section). The quality of the LCF was estimated by an *R*-factor parameter (*Rf*) of the following form: $\sum[y_{exp} - y_{calc}]^2 / \sum[y_{exp}]^2$.

Arsenic K-edge data were fit using a classical shell-by-shell analysis (e.g., (Morin et al., 2009)), with theoretical phase and amplitude functions calculated using the FEFF8.2 code (Akudinov et al., 1998) and scorodite ($FeAsO_4 \cdot 2H_2O$) (Hawthorne, 1976) and tooeleite ($Fe_6(AsO_3)_4SO_4(OH)_4 \cdot 4H_2O$) (Morin et al., 2007) as structural models for As(V) and As(III), respectively (Morin et al., 2008; Wang et al., 2008). The fit quality was estimated using a reduced χ^2 function with $N_{ind} = (2\Delta k \Delta R)/\pi$ or the number of independent parameters, where p is the number of free fit parameters, n is the number of data points fitted, k is the wave vector, and $\|FT\|_{exp}$ and $\|FT\|_{calc}$ are the experimental

and theoretical Fourier transform magnitudes within the *R*-range 2.2–3.6 Å. LCF analysis of the As K-edge data for BoFeN1 samples was also performed using experimental data at the As K-edge collected on the same set of model compounds used for Fe K-edge data analysis (see next section). Additional information on XRD, XANES, and EXAFS data acquisition and treatment is given as Supporting Information.

2.4. Model compounds

Fe K-edge EXAFS and XANES data from biogenic samples were analyzed by LCF using a large set of model compound spectra including ferrihydrite (Fh), goethite (Gt), hematite (Hm), lepidocrocite (Lp), akaganeite (Aka) as well as iron–arsenate and Fe–arsenite (Morin et al., 2003). The model compounds used for the best fits reported in the present study were: synthetic 4-Line ferrihydrite prepared following the controlled hydrolysis protocol from (Schwertmann et al., 1999) using a base addition rate of 67 μmol/min and a synthetic goethite (sample sch3-0) kindly provided by Prof. U. Schwertmann that was prepared via Fe(II) oxidation and Fe(III) hydrolysis at $T = 25$ °C (Goodman and Lewis, 1981). This goethite sample yielded the best XANES and EXAFS fits likely because it has a small Mean Coherent Domain size, i.e., $MCD_{110} = 11$ nm, $MCD_{001} = 15$ nm, which are close to those observed for our biogenic samples. As K-edge EXAFS data on Fe oxide phases produced by the Fe(II)-oxidizing strain BoFeN1 in the presence of either As(III) or As(V) were compared to EXAFS spectra from As(III) and As(V) adsorption and co-precipitation model samples, e.g., As(III) sorbed on Fh, Gt, and Lp, As(V) sorbed on Fh and Gt, As(III) co-precipitated with Fh and an amorphous As(III)/Fe(III) co-precipitate. Adsorption samples were prepared according to previously used methods (Ona-Nguema et al., 2005) and include: As(III) sorbed on ferrihydrite (As(III)/Fh) at surface coverages of 0.035, 0.22 and 0.89 μmol/m^2, As(III) sorbed on goethite (As(III)/Gt) at surface coverages of 0.035 and 0.85 μmol/m^2, As(III) sorbed on lepidocrocite (As(III)/Lp) at a surface coverage of 1.33 μmol/m^2, As(V) sorbed on ferrihydrite (As(V)/Fh) and goethite (As(V)/Gt) at surface coverages of 0.9 μmol/m^2. Co-precipitation samples prepared at pH 7 included As(III) co-precipitated with ferrihydrite (As(III)–Fh cpp) with an As/Fe molar ratio of 0.01 corresponding to a As(III) surface coverage of 0.22 μmol/m^2, and two amorphous As(III)–Fe(III) and As(V)–Fe(III) co-precipitates As(III)–Fe(III) cpp and As(V)–Fe(III) cpp, respectively, prepared at pH 7 with As/Fe molar ratios of 0.32 and 0.39, respectively, measured in the solid phase (Morin et al., 2003).

3. RESULTS AND DISCUSSION

3.1. Immobilization of As(III) and As(V) by the Fe(II)-oxidizer BoFeN1

After 8 days of incubation, 90.7–99.7% of the initially present dissolved Fe(II) (6–12 mM) was removed from solution, as determined by quantification of dissolved Fe(II) in the supernatant (Table S1, Fig. S1 as Supporting Information). Fe(III) concentration in the range of 0.0–1.1 mM could be detected in the dissolved fraction after 8 days probably present as colloids. The highest Fe(III) value (1.1 mM) was detected in the As(III) 500 μM set-up, lower As concentrations and As-free set-up yielded final Fe(III) concentrations between 0.0 and 0.6 mM (see Supporting Information S1). At the same time, more than 95% of the initially added As was associated with the solid phase as evidenced by the decrease in dissolved As concentrations, except for the experiment with the highest As(III) loading. In this case 87% of the initially present As was removed (Table S1). As(III) was not as efficiently immobilized (87–97%) as As(V) (96–98%) with increasing initial As concentrations resulting in decreasing fractions of immobilized As. These results are consistent with a previous study (Hohmann et al., 2010) where immobilization of As by strain BoFeN1 was higher than 96% at initial As concentrations <50 μM. Molar ratios of As:Fe in the solids calculated from the chemical composition of the supernatants (Table S1) ranged from 0.007 to 0.067 (Table 1). These values were similar for As(III) and As(V) and close to the initial As:Fe ratios, since the major fraction of the initially present Fe and As was present in the solid phase after Fe(II) oxidation in all experiments.

3.2. Mineralogy of the biogenic Fe-bearing mineral phases

X-ray powder diffraction analyses indicate that goethite is the only crystalline phase present in all of the biogenic samples studied (also in the presence of As), except for traces (<1 wt.%) of lepidocrocite detected in the 200 μM As(III) sample. Minor amounts of poorly crystalline components could not be identified using XRD since identification and quantification of disordered and/or nanocrystalline components such as ferrihydrite (Fh) are difficult to detect at low concentration in a solid phase mixture containing large amounts of crystalline goethite (Gt). Such quantification was especially difficult, even using Rietveld analysis, because of the overlap with the broad reflections arising from the glass capillary container used for powder XRD data collection. Rietveld analysis of the background-subtracted diffraction pattern (Fig. 1) indicated that goethite crystallites were of equi-dimensional shape with Mean Coherent Domain (MCD) values for the 1 1 0 plane (MCD_{110} values) between 11 and 18 nm and MCD_{001} values between 17 and 22 nm. It is remarkable that the MCD sizes of the goethite crystallites did not vary significantly as a function of As concentration in the samples (Table 1). In addition cell parameters of goethite in all samples studied ($a = 4.61 \pm 0.01$ Å; $b = 9.95 \pm 0.01$ Å; $c = 3.02 \pm 0.01$ Å in P*bnm* SG) were similar to those of pure goethite (Szytuła et al., 1968). Therefore, we conclude that the different As concentrations used in our experiments did not influence the MCD size (crystallite size) of the goethites formed during biogenic Fe(II) oxidation. However, SEM observations on similar samples reported by Hohmann et al. (2010) showed that, in the presence of arsenic, goethite particles tend to lose their acicular morphology and had smaller particle sizes. This difference between

Table 1
Mineralogical analysis of the solid samples after complete Fe(II) oxidation (after 8 days) by the nitrate-reducing Fe(II)-oxidizing strain BoFeN1. Results of linear least squares decomposition of the Fe K-edge XANES, EXAFS are given for the best fits that were obtained using microcrystalline goethite (Gt) and 4-Line ferrihydrite (Fh) as model compounds. Corresponding fits are reported in Figs. 2, S2 and S3. These results show a regular increase of the Fh fraction with increasing initial As concentration in the incubation experiments. MCD_{001} refers to the Mean Coherent Domain size of goethite along the *c*-axis (needle axis) in the P*bnm* space group, measured using Rietveld refinement of XRD patterns of the solid samples. MCD_{110} refers to MCD size along the orthogonal direction. MCD values indicate that the needle shape is not well developed for the goethite crystallites formed in our BoFeN1 experiments, which have almost equi-dimensional morphologies.

Sample	Molar ratio [As/Fe] in precipitates[a]	XANES			EXAFS			Gt–XRD	
		Gt (%)	Fh (%)	Sum	Gt (%)	Fh (%)	Sum	MCD_{110} (nm)	MCD_{001} (nm)
As-free	–	99 ± 2	<2	100 ± 1	87 ± 5	13 ± 5	100 ± 2	15	20
As(III) 50 μM	0.007 [0.003–0.007]	99 ± 1	<2	100 ± 1	88 ± 5	12 ± 5	100 ± 2	11	20
As(III) 200 μM	0.020 [0.015–0.020]	93 ± 3	7 ± 3	100 ± 1	89 ± 5	13 ± 5	102 ± 2	17	17
As(III) 500 μM	0.056 [0.018–0.063]	67 ± 5	34 ± 5	101 ± 2	n.m.	n.m.	n.m.	n.m.	n.m.
As(V) 50 μM	0.008 [0.001–0.008]	95 ± 3	5 ± 3	100 ± 1	86 ± 5	7 ± 5	93 ± 2	16	22
As(V) 200 μM	0.028 [0.007–0.028]	76 ± 5	24 ± 5	100 ± 1	59 ± 10	42 ± 10	101 ± 2	15	19
As(V) 500 μM	0.067 [0.010–0.070]	68 ± 5	32 ± 5	100 ± 1	51 ± 10	49 ± 10	100 ± 2	18	21

n.m.: not measured.
[a] For details of calculation of the molar ratios see Supporting Information S1.

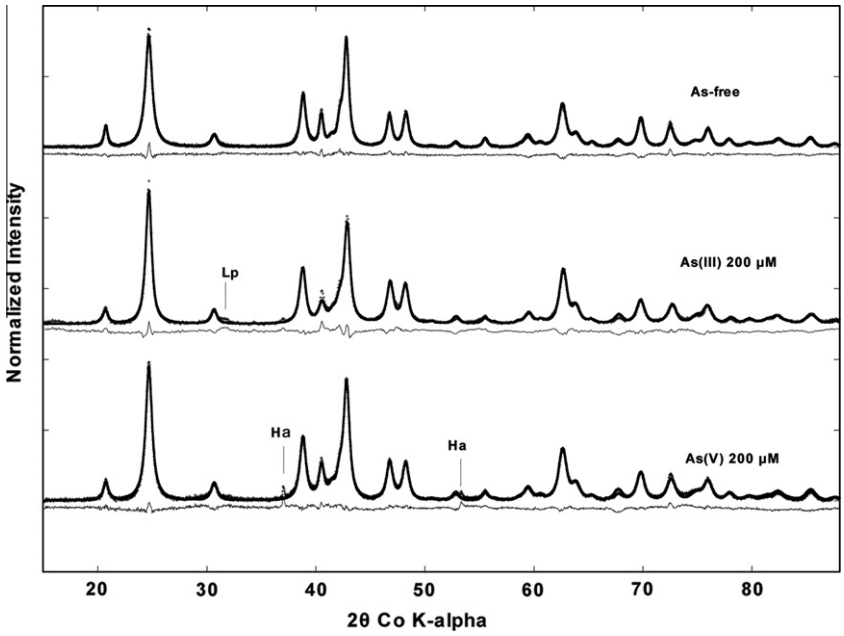

Fig. 1. Rietveld refinement of XRD powder patterns for selected Fe mineral samples produced by the Fe(II)-oxidizing strain BoFeN1 in the absence/presence of As. Experimental and calculated curves are displayed as dotted and solid lines, respectively. Goethite is the major phase in all samples. The MCD values of the goethite derived from this refinement procedure are reported in Table 1 for all samples studied. The potential presence of ferrihydrite could not be detected due to the intense background from the glass capillary container that has been subtracted. Lp: lepidocrocite (γ-FeOOH). Ha: halite (NaCl) precipitated upon drying. Changes in relative intensity of the low angle Bragg peaks are due to absorption effects through the glass capillary, with different amounts of powders for the different samples. Absorption corrections have been done accordingly using the formalism implemented in the XND code (Berar, 1990).

particle size and MCD size can be explained by the fact that acicular goethite particles are generally multi-domain particles (Cornell and Schwertmann, 2003). Such acicular morphology could be lost in the As containing samples, due to a dispersion of the small (10–20 nm) goethite domains.

XANES and EXAFS were used to identify and quantify the Fe-bearing phases in the biologically formed precipitates. Results are reported in Table 1 and selected fits are displayed in Fig. 2. The complete set of fits is reported in the Supporting Information (Figs. S2 and S3 for XANES and EXAFS data, respectively). For all samples, best fits were obtained by combining the XAS spectra of microcrystalline Sch3-0 goethite (Gt) and 4-Line ferrihydrite (Fh) (Fig. 2). Corresponding optimal *Rf* values ranged from

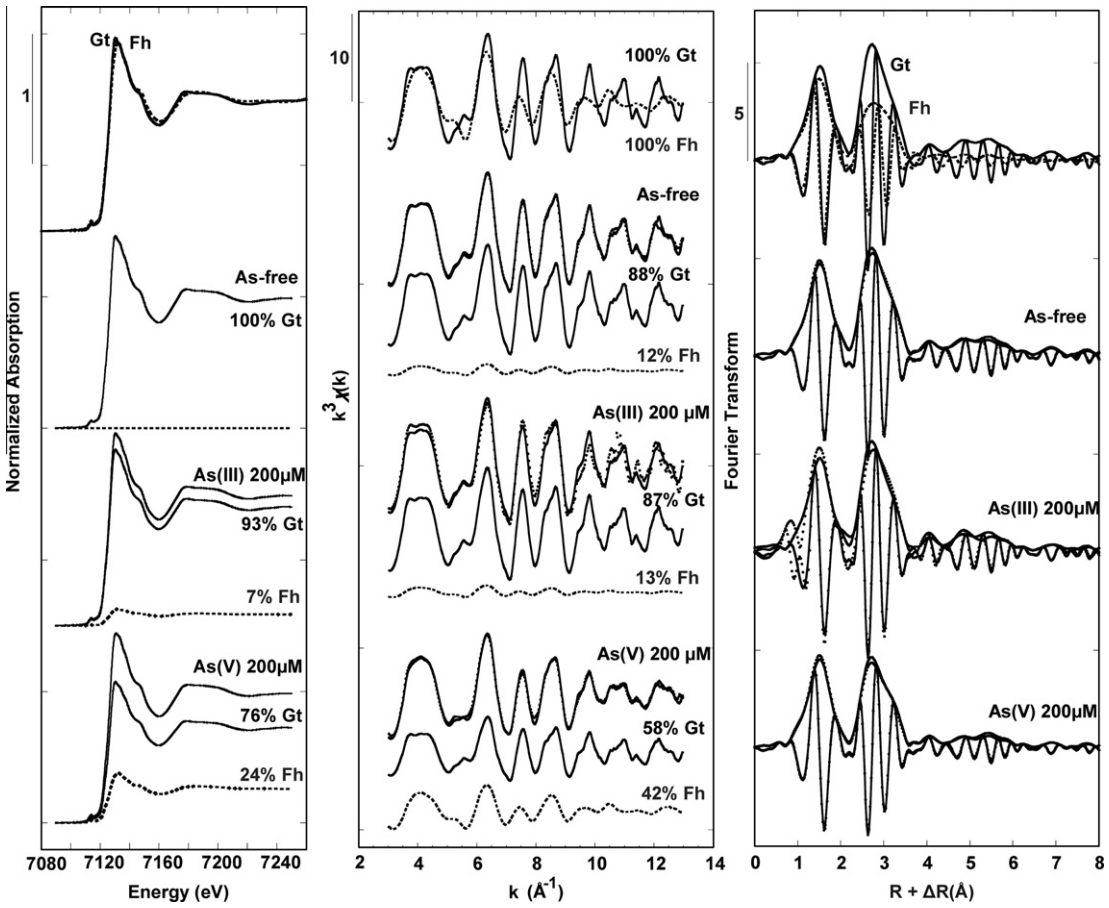

Fig. 2. Fe K-edge XANES data, k^3-weighted EXAFS data, and their Fourier transforms of the biogenic solids after 8 days, for selected samples, including As-free, As(III) 200 µM and As(V) 200 µM. Data were fit by linear combination least squares of experimental spectra from Gt and Fh model compounds. Note the difference in shape of the Gt and Fh XANES spectra, with a small peak at 7165 eV in the Gt spectrum. For each sample, the experimental and fitted curves are displayed as dotted and solid lines, respectively. For the XANES and k^3-weighted EXAFS, the fitting components are also displayed below each spectrum. The Fh component increases with increasing initial As concentration especially in the case of As(V) (see Table 1).

0.03 to 0.3 for XANES data and 0.008 to 0.03 for EXAFS data. Other compounds including lepidocrocite, hematite, akaganeite, amorphous iron–arsenite (As:Fe = 0.32) and iron–arsenate (As:Fe = 0.39) were below the detection limit of our LCF, i.e., typically 5% in XANES analysis and 15% in EXAFS analysis. Significantly lower quality fits, with more than 50% higher *Rf* values, were obtained when using highly crystalline goethite instead of the microcrystalline sch3-0 Gt sample mixed with Fh (data not shown). The variation among the fitting results obtained when using 2-Line, 4-Line or 6-Line ferrihydrite as a second component in a mixture with sch3-0 goethite was used to estimate standard deviation of individual components reported in Table 1. These variations were especially large when fitting EXAFS data because the amplitude of the second-neighbor signal in ferrihydrite Fe-K-edge EXAFS varies slightly as a function of the ferrihydrite variety. In contrast these variations in the fitting results were found to be much lower when fitting the XANES data. Consequently, for EXAFS, the standard deviations for the goethite and ferrihydrite components were as high as ±10%. A higher precision was obtained for the XANES results, with standard deviations lower than 5%, which indicates that percentages lower than ~15% were not significant in our EXAFS results.

From XANES LCF, we determined goethite as the main component of the biologically formed mineral precipitates (67–99 ± 2%). Ferrrihydrite is absent in the As-free sample and the proportion of goethite decreased regularly at the expense of the ferrihydrite proportion (5–34 ± 5%) for increasing As (As(III) as well as As(V)) concentrations (Fig. 2, Table 1). The contribution of the ferrihydrite component to the EXAFS of the As(III) 500 µM, As(V) 200 µM and As(V) 500 µM sample is illustrated by the decrease in amplitude of the k^3-weighted EXAFS spectra (Fig. 2), which is caused by a slight decrease in the contribution from second-neighbors as observed in the Fourier transform curves. It was noticeable that the ferrihydrite component is higher in biogenic solids from the As(V) experiments than in those from the As(III) experiments, except for the highest initial As concentration (500 µM). LCF analysis of the EXAFS data also yielded similar trends, but with lower accuracy and systematically higher fractions of the Fh component,

than for the XANES data decomposition (Table 1). This overestimation of the Fh component by EXAFS LCF can be explained by the nanocrystalline and poorly ordered character of Fh, which decreases the relative amplitude of its Fe–EXAFS spectrum compared to that of goethite.

Mössbauer spectroscopy analyses of a complementary series of ^{57}Fe doped As-free, As(III) 200 μM and As(V) 200 μM samples (Table S2 and Fig. S4 in Supporting Information) confirmed XRD and Fe K-edge EXAFS and XANES results. A goethite sextet was the dominant component in the Mössbauer spectra of these samples, with an average hyperfine field similar to that of pure goethite at 77 K (Isomer shift (IS) ~0.48 mm/s; Quadrupole shift (QS) ~−0.11 mm/s; Hyperfine field averaged (Hf) ~45 T, see also Supporting Information Table S2). In the As(V) 200 μM sample an additional Fe(III) doublet was observed at 77 K and 140 K that can be assigned to ferrihydrite, while it is absent in the As-free and As(III) 200 μM sample, in agreement with the trend observed in XANES and EXAFS data of the non-^{57}Fe-doped samples. However, the lower amount of Fh observed in the ^{57}Fe doped As(V) 200 μM sample (~7%), compared to our XANES and EXAFS results on the non-^{57}Fe-doped samples (24% and 42% respectively) can be explained by either aging of the Fh component (Cornell and Schwertmann, 2003) or a slow biotic re-reduction as described for the phototrophic Fe(II)-oxidizing strain SW2 in Kappler and Newman (2004) due to a longer incubation time of the precipitates.

Nevertheless, the present mineralogical analyses of BoFeN1 samples indicate that arsenite and arsenate can influence the identity of the neoformed biogenic mineral and that further analysis of the modes of As binding to these Fe(III) (oxyhydr)oxide phases was then required to understand the roles of As(III) and As(V) in these mineralogical changes.

3.3. Solubility of As bound to biogenic Fe (oxyhydr)oxides

According to available data on the solubility of As(V)-containing poorly crystalline Fe(III)-containing phases, e.g., Fh at pH 7 ((Cancès et al., 2008) and references therein), the dissolved concentration of As(V) depends directly on the As:Fe ratio. Under the conditions of the present experiments, which include the highest As:Fe ratio of 0.067 in the As(V) 500 μM sample (Table S1), the dissolved As concentration is expected to be below 22 ppb (0.3 μM), a value expected for an As:Fe ratio of 0.16 at pH 7 (Cancès et al., 2008). This value is much lower than the dissolved As concentration of ~2847 ppb (~38 μM) measured in the supernatant of the As(V) 500 μM experiment after 8 days of incubation (Table S1). Based on the large amount of the As-rich Fh-like phase in this sample (~35%; Table 1), the effective As:Fe ratio in this As-rich phase should not be higher than 0.1, which still would imply dissolved As concentrations below 22 ppb (0.3 μM). This discrepancy might be related to the centrifugation procedure applied in our experiments, which may not have led to a complete separation of the colloidal solids from the liquid phase (Mikutta et al., 2010); this could have led to an overestimation of the dissolved As fraction.

In the case of As(III), the final dissolved As concentrations measured in the supernatants are systematically higher than in the As(V) experiments and reach ~6968 ppb (~93 μM) in the As(III) 500 μM experiment. In a previous study by Kappler et al. (2005) a BET surface area of 158 m^2/g was determined for solid phases formed by BoFeN1. In the presence of As(III), assuming a surface area of ~70 m^2/g for Gt from MCD measurements by XRD and 600 m^2/g for Fh (Dixit and Hering, 2003), the estimated surface area for the As(III) 500 μM sample should be ~400 m^2/g. Based on this value, the As(III) surface coverage of this sample is ~1.2 $\mu mol/m^2$, which is expected to yield dissolved As(III) concentrations of ~247 ppb (3.3 μM) in abiotic systems (Dixit and Hering, 2003; Sverjensky and Fukushi, 2006). This expected value is much lower than the final As concentration of ~6968 ppb (~93 μM) measured in the supernatant of our As(III) 500 μM experiment. This discrepancy can be again explained by the presence of Fe- and As-containing colloidal phases in the analyzed supernatant.

3.4. Arsenic speciation in biogenic minerals

Arsenic speciation was investigated by XANES and EXAFS spectroscopy at the As K-edge in the biogenic samples collected after complete Fe(II) oxidation (Fig. 3). XANES data indicate that As(V) was not reduced during the incubation with BoFeN1, whereas As(III) was slightly oxidized, especially in the sample with the lowest As(III) loading (As(III) 50 μM). LCF of the XANES spectrum of this latter sample (data not shown) indicate that the fraction of As(V) did not exceed 10%, which could also be due to an abiotic oxidation process as shown previously in abiotic experiments for a mixture of goethite and Fe(II)-bearing phases (Amstaetter et al., 2009).

As K-edge EXAFS data exhibit weak second-neighbor contributions for both As(III) and As(V) samples indicating that As was not incorporated in the structure of any crystalline phase but rather formed inner-sphere surface complexes (Fig. 3). Shell-by-shell fit of the EXAFS data yield As–O distances fully consistent with the AsO_3 pyramid geometry in the As(III) samples (1.79 ± 0.02 Å) and with the AsO_4 tetrahedral geometry in the As(V) samples (1.69 ± 0.02 Å). Second-neighbor contributions were best fit with a combination of two Fe shells at distances of 2.9 and 3.4 ± 0.02 Å for the As(III) samples (Table 2), and with one Fe shell at a distance of 3.3 ± 0.02 Å for As(V) samples (Table 3).

The presence of two Fe shells around As for the biogenic Fe minerals containing As(III) is illustrated by the weak beat pattern around $k = 10$ Å^{-1} in the back-Fourier transform of the second neighbor peak, k being the wave vector of the photoelectron (Fig. S5). This beat pattern is more pronounced in the spectrum of As(III) adsorbed on 2-Line ferrihydrite (As(III)/Fh), whereas it is absent in the spectrum of As(III) sorbed on goethite (As(III)/Gt). For As(III)/Fh, the beat pattern is associated with the presence of two Fe shells at 2.9 and 3.4 Å whereas the absence of a beat pattern for As(III)/Gt is associated with a single Fe-shell at a distance of 3.3 Å (Fig. 4), as for As(III)/Lp

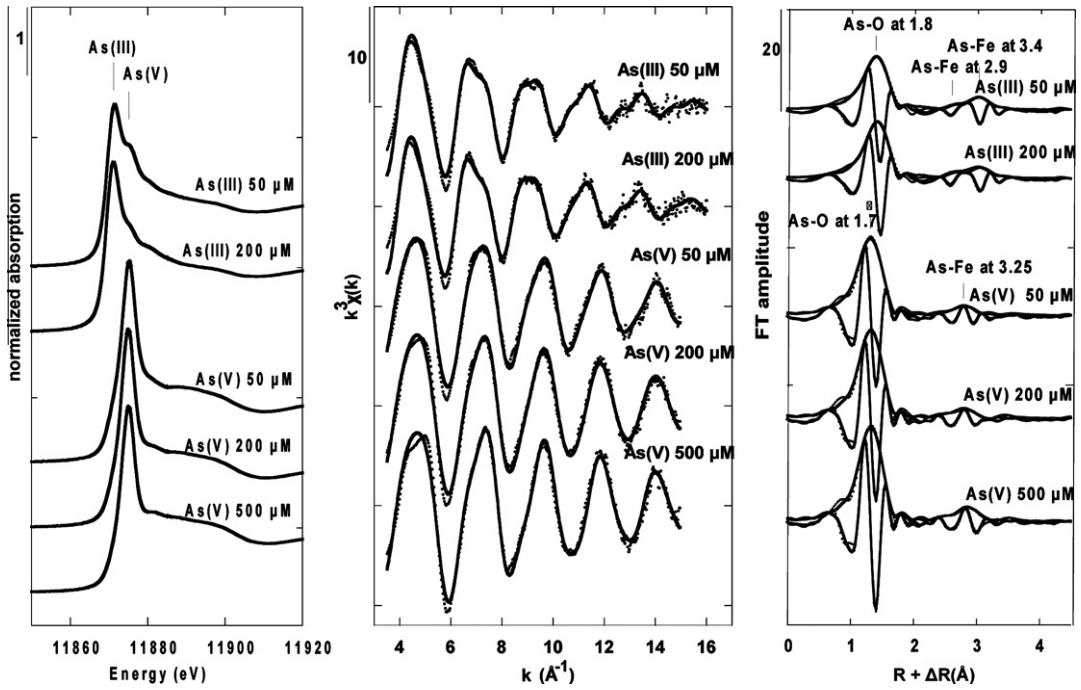

Fig. 3. As K-edge XANES data, k^3-weighted EXAFS data and their Fourier Transform of the biogenic solids after 8 days, for all samples analyzed. Data were fit using a classical shell-by-shell analysis, including multiple scattering within the first oxygen shell (see text and Table 2). For each sample, the experimental and fitted curves are displayed as dotted and solid lines, respectively. The local environment around As(III) includes two As–Fe distances (Table 2) indicated by a beat pattern in the back-Fourier transform of the second-neighbor contribution (Fig. S5). This environment differs from that around As(V), which includes only one As–Fe distance (Table 3).

(Figs. 3, 4, and S5; Table 2). This characteristic As–Fe distance of 3.3 Å for As(III) sorbed on goethite was also obtained by Manning (2002) with EXAFS data similar to those obtained in the present study and by Ona-Nguema et al. (2005) (Figs. 4 and S5). According to Ona-Nguema et al. (2005), these differences between As(III) surface complexes on Fh, Gt and Lp, can be attributed to the presence of both bidentate edge-sharing complexes (^2E) and bidentate corner-sharing complexes (^2C) for As(III)/Fh corresponding to As–Fe pairs at 2.9 and 3.4 Å, respectively. Mostly ^2C complexes with an As–Fe pair at 3.3 Å have been proposed in the case of As(III)/Gt and As(III)/Lp (Manning et al., 1998; Manning, 2002; Ona-Nguema et al., 2005). In spite of these differences between the As(III) adsorption complexes found on these substrates, the present EXAFS analysis did not lead to an unambiguous conclusion about the nature of the As(III) immobilization mechanism in the BoFeN1 samples. Indeed, although the As–Fe distances in the BoFeN1 samples are similar to those found for As(III)/Fh sorption and co-precipitation samples (2.9 and 3.4 Å), the relative proportion of the two contributions of the two Fe shells differs in BoFeN1 samples and in As(III)/Fh model compounds (Table 2 and Figs. 4 and S5). More precisely, the relative contribution from the longest As–Fe distance (3.4 Å) is significantly higher for the BoFeN1 samples than for As(III)/Fh sorption and co-precipitation samples (Figs. 4 and S5), regardless of the surface coverage or As:Fe ratio investigated (Table 2, Fig. 4). Accordingly, LCF analysis of the BoFeN1 As K-edge EXAFS data showed that the spectra of both the As(III) 50 and 200 µM cannot be perfectly reproduced by a combination of As(III) sorbed on Fh and As(III) sorbed on Gt, whatever As:Fe ratio chosen for these model compounds (Fig. S6). Including other model compounds such as As(III) co-precipitated with Fe(III) did not improve the LCF results. This discrepancy comes from the fact that the contribution of the As–Fe distance at 3.4 Å in the biogenic samples is stronger than in the spectra of our abiotic As(III)/Fh sorption and co-precipitation model compounds. Indeed, Fig. 4 and Table 2 show that As(III)–Fe(III) co-precipitation model compounds yield stronger contribution at 2.9 Å than the BoFeN1 samples. This strong contribution at 3.4 Å cannot be accounted for by the As(III)/Gt sorption model compound, for which the dominant As–Fe distance is at 3.3 Å. For As(III) adsorption on Fh, the As–Fe distance at 3.4 Å is generally attributed to ^2C double corner-sharing As(III) surface complexes, while the As–Fe distance at 2.9 Å is assigned to ^2E edge-sharing As(III) surface complexes. The unusual strong contribution at 3.4 Å observed in the BoFeN1 samples can be related to an increase of the relative proportion of ^2C over ^2E As(III) complexes at the surface of Fh. Although this difference with abiotic model compounds is not yet explained, we hypothesize that it could be related to a change in the surface structure or reactivity of Fh in the presence of BoFeN1, since microbial exopolymers could act as competitors for As surface sorption (as shown for carboxylates that influence the coordination of As(V)-binding to ferrihydrite (Mikutta et al., 2010)). Nevertheless, LCF analysis of As K-edge data for the As(III) BoFeN1 samples suggests

Table 2
Results of shell-by-shell fitting of unfiltered EXAFS data at the As K-edge for the As(III) samples studied. Fit results for BoFeN1 samples (As(III) 50 μM and As(III) 200 μM) are compared with those for model compounds including As sorption and co-precipitation samples (cpp) (see text). R (Å): interatomic distances; N: number of neighbors; σ (Å): Debye Waller factor, ΔE_0 (eV): difference between the experimentally determined threshold energy and the FEFF8-calculated threshold energy without using the self-consistent potential option for faster calculations, which explains the high ΔE_0 values; χ^2FT: Goodness of fit (see text). During the fitting procedure, all parameter values indicated by (–) were linked to the parameter value placed above in the table. The N parameter of the As–O–O (AsO_3) multiple scattering path was fixed to 6.0 (f). Standard deviations were estimated from the fit of the tooeleite As K-edge EXAFS data (not shown). Fit results for the BoFeN1 samples are reported in Fig. 3 and are compared with model compound data in Fig. 4. Fitting results for Fourier filtered data within the 2.3–3.5 Å R-range are presented for BoFeN1 samples and for selected model compounds (Ona-Nguema et al., 2005) in Fig. S5 and fall within the estimated standard deviations reported in the table.

Sample	Path	R (Å) (±0.02)	N (± 0.2)	σ (Å) (±0.01)	ΔE_0 (eV) (±3)	$\chi^2 FT$
As(III)/Gt 0.85 μmol/m^2 (Ona-Nguema et al., 2005)	As–O	1.76	3.1	0.07	15	0.09
	As–O–O	3.20(f)	6.0(f)	–	–	
	As–Fe	3.31	1.7	0.09	–	
As(III)/Lp 0.85 μmol/m^2 (Ona-Nguema et al., 2005)	As–O	1.76	3.1	0.07	16	0.11
	As–O–O	3.20(f)	6.0(f)	–	–	
	As–Fe	3.34	0.9	0.09	–	
As(III)/Fh 0.035 μmol/m^2	As–O	1.79	2.8	0.05	17	0.09
	As–O–O	3.20(f)	6.0(f)	–	–	
	As–Fe	2.94	0.4	0.06	–	
	As–Fe	3.41	0.6	–	–	
As(III)/Fh 0.22 μmol/m^2 (Ona-Nguema et al., 2005)	As–O	1.78	3.1	0.06	17	0.10
	As–O–O	3.20(f)	6.0(f)	–	–	
	As–Fe	2.93	0.4	0.06	–	
	As–Fe	3.42	0.4	–	–	
As(III)/Fh 0.89 μmol/m^2 (Ona-Nguema et al., 2005)	As–O	1.76	3.0	0.07	18	0.11
	As–O–O	3.20(f)	6.0(f)	–	–	
	As–Fe	2.93	0.7	0.09	–	
	As–Fe	3.42	0.7	–	–	
As(III)–Fh cpp, As:Fe = 0.01, 0.22 μmol/m^2	As–O	1.76	3.1	0.07	19	0.11
	As–O–O	3.20(f)	6.0(f)	–	–	
	As–Fe	2.95	0.5	0.07	–	
	As–Fe	3.44	0.4	–		
As(III)–Fe(III) cpp, As:Fe = 0.32 (Morin et al., 2003)	As–O	1.79	2.8	0.06	20	0.10
	As–O–O	3.20(f)	6.0(f)	–	–	
	As–Fe	2.95	0.4	0.08	–	
	As–Fe	3.38	0.9	–	–	
As(III) 50 μM	As–O	1.77	3.4	0.08	17	0.09
	As–O–O	3.20(f)	6.0(f)	–	–	
	As–Fe	2.93	0.2	0.08	–	
	As–Fe	3.39	1.0	–	–	
As(III) 200 μM	As–O	1.77	3.2	0.07	18	0.09
	As–O–O	3.20(f)	6.0(f)	–	–	
	As–Fe	2.94	0.3	0.08	–	
	As–Fe	3.40	1.2	–	–	

that As(III) preferentially adsorbs at the surface Fh relatively to Gt, the estimated proportion of As(III) sorbed to Fh being 75% and 50% for the As(III) 50 and 200 μM samples (Fig. S6). With regard to As(V) BoFeN1 samples, EXAFS analysis indicates a single As–Fe distance of 3.2–3.3 Å (Table 3, Figs. 3 and 5). This distance is similar to that classically found for As(V) adsorbed to Gt and other FeOOH polymorphs (Waychunas et al., 1993; Fendorf et al., 1997; Foster et al., 1998) as well as for As(V) adsorbed or co-precipitated with Fh (Waychunas et al., 1993; Foster et al., 1998; Cancès et al., 2005; Paktunc et al., 2008). It is generally attributed to bidentate ^2C complexes (Waychunas et al., 1993; Sherman and Randall, 2003). However, due to the similarity among the EXAFS spectra for As(V) adsorbed on 2-Line ferrihydrite and on goethite, and co-precipitated with Fe(III) at high As loading (Cancès et al., 2005; Paktunc et al., 2008; Fig. 5, Table 3), the present EXAFS analysis at the As K-edge did not allow us to distinguish between Gt and Fh as sorbents for As(V) in the biogenic solid phases produced by BoFeN1.

Altogether, our As K-edge EXAFS results indicated that both As(III) and As(V) formed inner-sphere complexes at the surface of the biogenic ferric (oxyhydr)oxides produced by BoFeN1. However, our data do not preclude

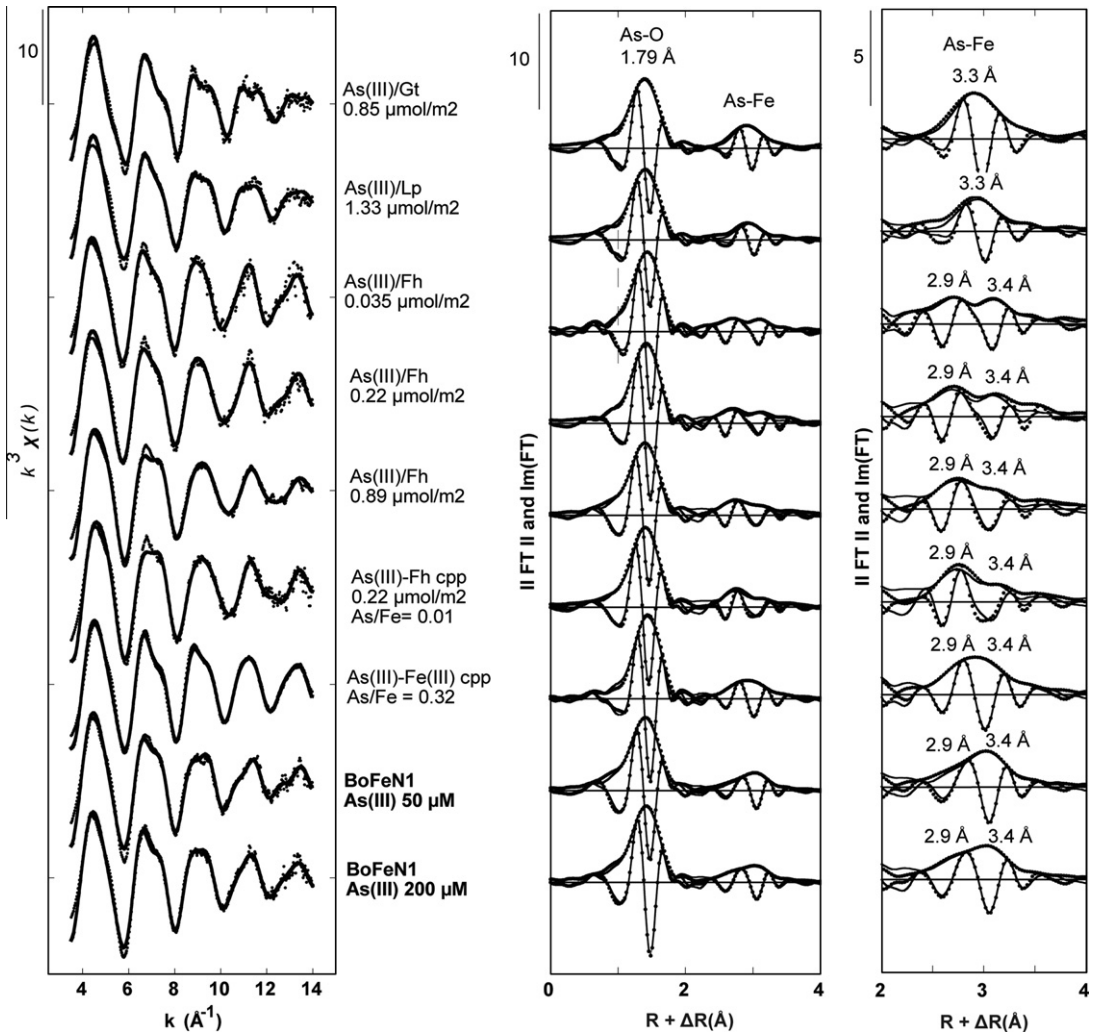

Fig. 4. Comparison of As K-edge EXAFS data for As(III) BoFeN1 samples and for As(III)-sorption samples on goethite and ferrihydrite. Second neighbor contributions are fit using As–Fe pair at a distance of 3.3 Å and a multiple scattering paths within the AsO_3 pyramid. Experimental and fit curves are displayed as dotted and solid lines respectively. Fitting results are reported in Table 2.

the presence of outer-sphere As surface complexes, since those are difficult to determine by EXAFS analysis because they are characterized by the lack of second-neighbor contribution. In particular, it can be noticed that the amplitude of the second neighbor contribution to the EXAFS of As(V) BoFeN1 samples (Fig. 5), and the corresponding number of Fe neighbors (Table 3), are systematically lower than those observed for the abiotic model compounds. Such difference could be possibly explained by an increasing proportion of As(V) outer-sphere surface complexes in the biogenic BoFeN1 samples relative to pure As–Fh model compounds, as recently proposed by Mikutta et al. (2010) for As(V) sorption on Fh in the presence of citrate. Indeed, biogenic BoFeN1 samples are also expected to contain organic moieties interacting with the surface of Fh. Association of organic molecules, especially exopolysaccharides, with poorly ordered extracellular Fe–phosphates produced by strain BoFeN1 has recently been found by Miot et al. (2009) as well as for As–Fe(III)-bearing biominerals in an acid mine drainage (Benzerara et al., 2008). Carbon-containing moieties associated with these organic molecules could indeed compete with As(V) and As(III) for complexation on the Fe–OH surface sites and could thus explain the differences observed between the As surface complexes in BoFeN1 samples and in abiotic analogs. Similar competition between organics and As has been described for humic and fulvic acids (Sharma et al., 2010).

High-resolution transmission electron microscopy–energy dispersive X-ray spectroscopy (HRTEM–EDXS) using a focused electron beam of a few nanometers in size yielded further information on As distribution at the nanoscale in the biogenic samples. Although statistically significant results would require more systematic analyses, EDXS data obtained on selected spots on sample As(III) 200 µM indicated that As(III) is uniformly distributed over the sample matrix.

An example of a HRTEM image of this sample is given in Fig. S7A. This microphotograph was chosen because it displays a poorly crystalline Fe-containing material in association with crystalline particles. This poorly crystalline

Table 3
Results of shell-by-shell fitting of unfiltered As K-edge EXAFS data for the As(V) samples studied. BoFeN1 samples (As(V) 50 μM, As(V) 200 μM and As(V) 500 μM) are compared with model compounds samples including As(V) sorbed on goethite and ferrihydrite as well as As(V) coprecipitated with Fe(III) (see text). R (Å): interatomic distances; N: number of neighbors; σ (Å): Debye Waller factor, ΔE_0 (eV): difference between the experimentally determined threshold energy and the FEFF8-calculated threshold energy without using the self-consistent potential option, for faster calculations; χ^2FT: Goodness of fit (see text). During the fitting procedure, all parameter values indicated by (–) were linked to the parameter value placed above in the table. The N parameter of the As–O–O (AsO_4) multiple scattering path was fixed at 12.0 (f). Standard deviations were estimated from the fit of scorodite As K-edge EXAFS data (not shown). Fit results for these BoFeN1 samples are reported in Fig. 3 and are compared with model compound data in Fig. 5.

Sample	Path	R (Å) (±0.02)	N (±0.5)	σ (Å) (±0.01)	ΔE_0 (eV) (±3)	χ^2FT
As(V) 50 μM	As–O	1.69	4.1	0.06	0	0.16
	As–O–O	3.09	12.0(f)	–	–	
	As–Fe	3.24	0.4	0.05	–	
As(V) 200 μM	As–O	1.68	4.0	0.05	2	0.17
	As–O–O	3.10	12.0(f)	–	–	
	As–Fe	3.27	0.9	0.09	–	
As(V) 500 μM	As–O	1.68	4.2	0.05	2	0.22
	As–O–O	3.08	12.0(f)	–	–	
	As–Fe	3.28	1.0	0.08	–	
As(V)/Gt 0.8 μmol/m^2	As–O	1.68	4.0	0.07	5	0.16
	As–O–O	3.08	12.0(f)	–	–	
	As–Fe	3.29	0.8	0.07	–	
As(V)/Fh 0.9 μmol/m^2	As–O	1.69	4.1	0.05	5	0.15
	As–O–O	3.07	12.0(f)	–	–	
	As–Fe	3.30	1.4	0.09	–	
As(V)–Fe(III) As:Fe = 0.39	As–O	1.69	4.1	0.05	8	0.12
	As–O–O	3.09	12.0(f)	–	–	
	As–Fe	3.30	1.9	0.09	–	

component that accounts for a significant proportion of the solid phase in the area displayed in Fig. S7A was however scarcely observed over the studied HRTEM grid, in agreement with the low proportion of Fh found in this 200 μM sample (<10% as indicated by Fe K-edge XANES analysis; Table 1). EDXS analysis indicate that the As in the As(III) set-ups is homogeneously distributed over the sample including both the crystalline particles and the scarce areas of disordered material. HRTEM observations of the 200 μM As(V) sample (Figs. S7B and S8) significantly contrast with those of the 200 μM As(III) sample, and reveal that As(V) is preferentially bound to poorly crystalline mineral phase. Indeed, EDXS analyses of the poorly crystalline Fe (oxyhydr)oxide areas, yield systematically higher As:Fe intensity ratios for the X-ray K emission lines than for the goethite particles (Fig. S8). HRTEM–EDXS results are thus consistent with As K-edge EXAFS results that suggested As(III) adsorption onto both Fh and Gt. In addition, the association of As(V) with the poorly crystalline phase observed by HRTEM is consistent with the formation of an As-rich Fh phase that cannot be easily distinguished from a ferric-arsenate, i.e., amorphous As(V)–Fe(III) (oxyhydr)oxide, on the sole basis of EXAFS data at the As K-edge (Fig. S6; Table 3; Paktunc et al., 2008). Although it has been shown by these authors that ferric arsenate could be distinguished from Fh using EXAFS spectroscopy at the Fe K-edge, this distinction could not be made in the present study because the Gt spectrum dominates the EXAFS signal from our sample.

3.5. Influence of As on biogenic Fe(III) phases

The mineralogy of the Fe mineral precipitates formed by the nitrate-reducing Fe(II)-oxidizing strain BoFeN1 and probably also by other Fe(II)-oxidizing bacteria is strongly influenced by the composition of the growth medium (Miot et al., 2009; Larese-Casanova et al., 2010). In comparison to the study of Miot et al. (2009), which showed the formation of Fe-phosphate minerals by BoFeN1 in the absence of As, our study used a medium with a reduced phosphate content in order to avoid competition of phosphate sorption with As, especially to avoid competition of phosphate with As(V) for binding sites on the mineral surfaces. In the presence of As(III) with an As:Fe molar ratio below 0.02, strain BoFeN1 produced minerals of the same identity as in the absence of As – mainly goethite ($\geqslant$90%) – but the morphology was different. SEM investigations recently reported by Hohmann et al. (2010) showed that the Gt particles formed in the presence of As(III) are smaller and do not exhibit the needle-shaped morphology that were observed in the absence of As(III) (Kappler et al., 2005). These differences in particle size and morphology are not related to differences in MCD sizes since the present XRD data on similar samples indicate that this parameter is not influenced by the presence of As(III). One may thus infer that As(III) sorption at the surface of Gt particles tends to inhibit the aggregation of small Gt crystallites to form multi-domain Gt particles with the needle-shaped morphology classically observed for Gt (Cornell and Schwertmann, 2003).

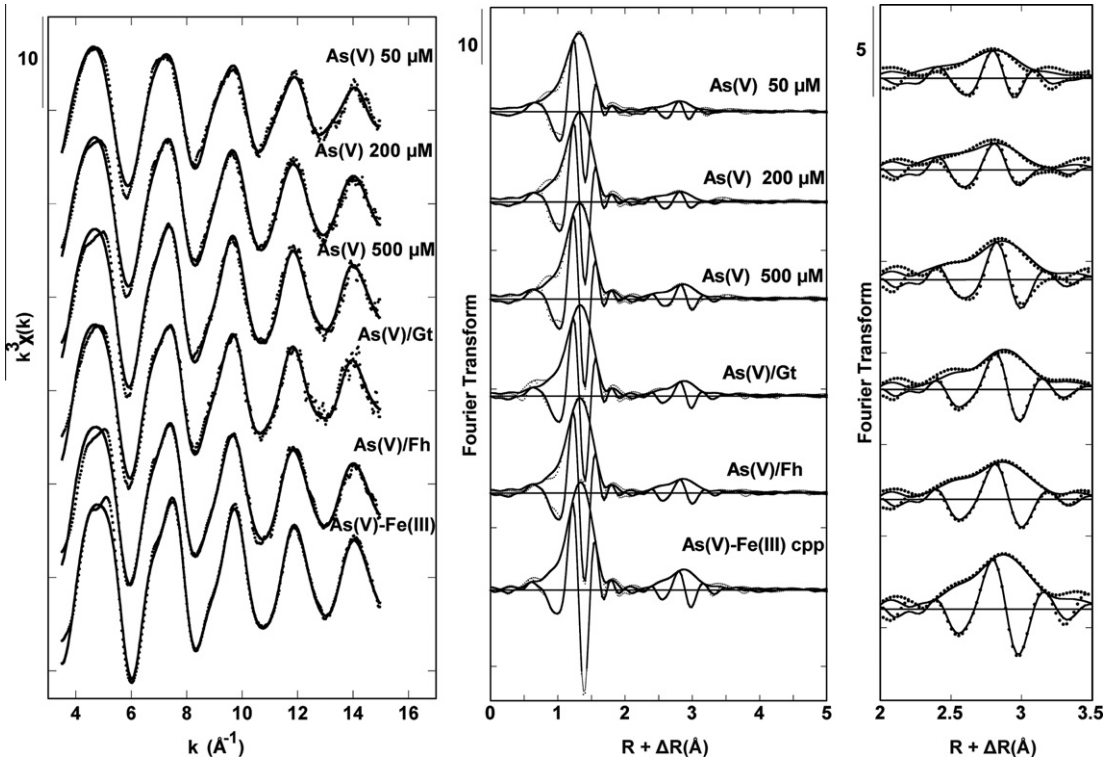

Fig. 5. Comparison of As K-edge EXAFS data for As(V) BoFeN1 samples and for As(V)-sorption samples on goethite and 2-Line ferrihydrite at As surface coverage of 0.8 and 0.9 µmol/m^2, respectively, and for an As(V)–Fe(III) amorphous co-precipitate with As:Fe = 0.39 mol/mol. Second neighbor contributions are fit using As–Fe pair at a distance of 3.25 ± 0.05 Å and a multiple scattering path within the AsO_4 tetrahedron. A detail of the FT of the second neighbor contribution is given on the right. Experimental and fit curves are displayed as dotted and solid lines respectively. Fitting results are reported in Table 3.

In the presence of As(V), a significant proportion of Fh (up to ~35%; Table 1) is produced in association with Gt, which emphasizes the role of As(V) in inhibiting the formation of goethite. This process is known for phosphate, which interferes with the nucleation and growth stages of Gt during the transformation of Fh to Gt (Shaw et al., 2005). A similar strong affinity of As(V) for Fe(III) has been recently reported for phosphate upon co-precipitation with Fh, which leads to the formation of amorphous phosphate in a mixture with Fh (Voegelin et al., 2010). The formation of amorphous Fe(III) phosphate phases was also reported upon oxidation of Fe(II) by BoFeN1 in the presence of a higher phosphate concentration (Miot et al., 2009). In the same way, upon co-precipitation with Fe(III), arsenate ions are known to inhibit edge-sharing polymerization of Fe(III) octahedra, leading to the formation of amorphous phases that can be even less ordered than ferrihydrite when the As(V):Fe molar ratio exceeds 0.25 at pH ⩽ 4.5 (Paktunc et al., 2008). Owing to the decrease and increase of Fe(III) and As(V) solubilities, respectively, from pH 4.5 to 7.0 (Cancès et al., 2008; Paktunc and Bruggeman, 2010) a weaker interaction between Fe(III) and As(V) is expected at pH 7 in the present study. However, in spite of the low As(V):Fe molar ratio (⩽0.067) used here, the formation of goethite is partially inhibited, and an As(V)-bearing ferrihydrite component forms in association with Gt. The present study thus shows that the binding modes of As to ferric minerals produced by biogenic oxidation of Fe(II) differ for As(III) and As(V) on the nanometer and molecular scales. This difference can be related to the high affinity of As(V) for Fe(III), which favor the formation of poorly ordered Fe (oxyhydr)oxide phases in association with Gt, even at an As(V):Fe molar ratio below 0.067. In contrast, although As(III) is known to sorb as efficiently as As(V) at the surface of most Fe-minerals at neutral pH (Dixit and Hering, 2003), we have shown that As(III) interferes less than As(V) with the nucleation and growth of Gt for the two lowest As concentrations investigated (50 and 200 µM). This is evidenced by the lower amount of Fh-like material formed in these As(III) experiments compared to the As(V) ones (Table 1). This observation of less influence of As(III) on Fe-oxide formation was previously observed in the case of As(III) co-precipitation with magnetite (Wang et al., 2008), for which As(III):Fe molar ratios higher than 0.067 were required to produce detectable amounts of poorly crystalline As–Fe precipitates.

ACKNOWLEDGEMENTS

This work was supported by a research proposal (KA 1736/14-1) from the German Research Foundation (DFG) and by the project "MicroActiv" of the BMBF/DFG program "Geotechnologien" to AK, and by a BMBF IPSWaT fellowship to CH. The work done by GM was funded by EC2CO-CYTRIX CNRS/INSU program, by ACI/FNS grant #3033, and by SESAME IdF grant #1775. Support was also provided by NSF grant CHE-0431425 (Stanford Molecular Environmental Science Institute). We would

like to thank Phil Larese-Casanova and Urs Dippon for Mössbauer spectroscopy measurements and Dr. Jörn Breuer (LAChemie Universität Hohenheim) and Dr Birgit Daus (Helmholtz-Zentrum für Umweltforschung GmbH - UFZ Leipzig) for ICP-MS analysis.

APPENDIX A. SUPPLEMENTARY DATA

Supplementary data associated with this article can be found, in the online version, at doi:10.1016/j.gca.2011.02.044.

REFERENCES

Akudinov A. L., Ravel B., Rehr J. J. and Condradson S. D. (1998) Real-space multiple scattering calculation and interpretation of X-ray absorption near-edge structure. *Phys. Rev. B* **58**, 7565–7576.

Amstaetter K., Borch T., Larese-Casanova P. and Kappler A. (2009) Redox transformation of arsenic by Fe(II)-activated goethite (α-FeOOH). *Environ. Sci. Technol.* **44**, 102–108.

Auffan M., Rose J., Proux O., Borschneck D., Masion A., Chaurand P., Hazemann J.-L., Chaneac C., Jolivet J.-P., Wiesner M. R., Van Geen A. and Bottero J.-Y. (2008) Enhanced adsorption of arsenic onto maghemites nanoparticles: As(III) as a probe of the surface structure and heterogeneity. *Langmuir* **24**, 3215–3222.

Benzerara K., Morin G., Yoon T. H., Miot J., Tyliszczak T., Casiot C., Bruneel O., Farges F. and Brown, Jr., G. E. (2008) Nanoscale study of As biomineralization in an acid mine drainage system. *Geochim. Cosmochim. Acta* **72**, 3949–3963.

Berar J. F. (1990) Reduction of the number of parameters in real time Rietveld refinement. *IUCr Sat. Meeting Powder Diffraction*. Toulouse.

Buswell A. M. (1943) War problems in analysis and treatment. *J. Am. Water Works Ass.* **35**, 1303.

Cancès B., Juillot F., Morin G., Laperche V., Alvarez L., Proux O., Hazemann J. L., Brown, Jr., G. E. and Calas G. (2005) XAS evidence of As(V) association with iron oxyhydroxides in a contaminated soil at a former arsenical pesticide processing plant. *Environ. Sci. Technol.* **39**, 9398–9405.

Cancès B., Juillot F., Morin G., Laperche V., Polya D., Vaughan D. J., Hazemann J. L., Proux O., Brown, Jr., G. E. and Calas G. (2008) Changes in arsenic speciation through a contaminated soil profile: a XAS based study. *Sci. Total Environ.* **397**, 178–189.

Catalano J. G., Park C., Fenter P. and Zhang Z. (2008) Simultaneous inner- and outer-sphere arsenate adsorption on corundum and hematite. *Geochim. Cosmochim. Acta* **72**, 1986–2004.

Chaudhuri S. K., Lack J. G. and Coates J. D. (2001) Biogenic magnetite formation through anaerobic biooxidation of Fe(II). *Appl. Environ. Microb.* **67**, 2844–2848.

Cornell R. M. and Schwertmann U. (2003) *The Iron Oxides – Structures, Properties, Reactions, Occurences and Uses*. Wiley-VCH Verlag, Weinheim.

Dixit S. and Hering J. G. (2003) Comparison of arsenic(V) and arsenic(III) sorption onto iron oxide minerals: implications for arsenic mobility. *Environ. Sci. Technol.* **37**, 4182–4189.

Egal M., Casiot C., Morin G., Parmentier M., Bruneel O., Lebrun S. and Elbaz-Poulichet F. (2009) Kinetic control on the formation of tooeleite, schwertmannite and jarosite by acidithiobacillus ferrooxidans strains in an As(III)-rich acid mine water. *Chem. Geol.* **265**, 432–441.

Fendorf S., Eick M. J., Grossl P. and Sparks D. L. (1997) Arsenate and chromate retention mechanisms on goethite.1. Surface structure. *Environ. Sci. Technol.* **31**, 315–320.

Foster A. L., Brown, Jr., G. E., Tingle T. N. and Parks G. A. (1998) Quantitative arsenic speciation in mine tailings using X-ray absorption spectroscopy. *Am. Mineral.* **83**, 553–568.

Goodman B. A. and Lewis D. G. (1981) Mössbauer spectra of aluminous goethites (alpha-FeOOH). *Eur. J. Soil Sci.* **32**, 351–364.

Hawthorne F. C. (1976) The hydrogen positions in scorodite. *Acta Crystallogr.* **B32**, 2891–2892.

Hegler F., Posth N. R., Jiang J. and Kappler A. (2008) Physiology of phototrophic iron(II)-oxidizing bacteria-implications for modern and ancient environments. *FEMS Microbiol. Ecol.* **66**, 250–260.

Hohmann C., Winkler E., Morin G. and Kappler A. (2010) Anaerobic Fe(II)-oxidizing bacteria show As resistance and immobilize As during Fe(III) mineral precipitation. *Environ. Sci. Technol.* **44**, 94–101.

Kappler A. and Newman D. K. (2004) Formation of Fe(III)–minerals by Fe(II)-oxidizing photoautotrophic bacteria. *Geochim. Cosmochim. Acta* **68**, 1217–1226.

Kappler A. and Straub K. L. (2005) Geomicrobiological cycling of iron. *Rev. Mineral. Geochem.* **59**, 85–108.

Kappler A., Schink B. and Newman D. K. (2005) Fe(III) mineral formation and cell encrustation by the nitrate-dependent Fe(II)-oxidizer strain BoFeN1. *Geobiology* **3**, 235–245.

Larese-Casanova P., Haderlein S. B. and Kappler A. (2010) Biomineralization of lepidocrocite and goethite by nitrate-reducing Fe(II)-oxidizing bacteria: effect of pH, bicarbonate, phosphate, and humic acids. *Geochim. Cosmochim. Acta* **74**, 3721–3734.

Manning B. A. (2002) Arsenic(III) oxidation and arsenic(V) adsorption reactions on synthetic birnessite. *Environ. Sci. Technol.* **36**, 976.

Manning B. A., Goldberg S. and Fendorf S. E. (1998) Surface structures and stability of arsenic(III) on goethite: spectroscopic evidence for inner-sphere complexes. *Environ. Sci. Technol.* **32**, 2383–2388.

Meng X., Korfiatis G. P., Christodoulatos C. and Bang S. (2001) Treatment of arsenic in Bangladesh well water using a household co-precipitation and filtration system. *Water Res.* **35**, 2805–2810.

Mikutta C., Frommer J., Voegelin A., Kaegi R. and Kretzschmar R. (2010) Effect of citrate on the local Fe coordination in ferrihydrite, arsenate binding, and ternary arsenate complex formation. *Geochim. Cosmochim. Acta* **74**, 5574–5592.

Miot J., Benzerara K., Morin G., Kappler A., Bernard S., Obst M., Férard C., Skouri-Panet F., Guigner J.-M., Posth N., Galvez M., Brown, Jr, G. E. and Guyot F. (2009) Iron biomineralization by anaerobic neutrophilic iron-oxidizing bacteria. *Geochim. Cosmochim. Acta* **73**, 696–711.

Morin G. and Calas G. (2006) Arsenic in soils, mine tailings, and former industrial sites. *Elements* **2**, 97–101.

Morin G., Juillot F., Casiot C., Bruneel O., Personné J.-C., Elbaz-Poulichet F., Leblanc M., Ildefonse P. and Calas G. (2003) Bacterial formation of tooeleite and mixed arsenic(III) or arsenic(V)–iron(III) gels in the carnoulès acid mine drainage, France. A XANES, XRD, and SEM study. *Environ. Sci. Technol.* **37**, 1705–1712.

Morin G., Rousse G. and Elkaim E. (2007) Crystal structure of tooeleite, $Fe_6(AsO_3)_4SO_4(OH)_4{\cdot}4H_2O$, a new iron arsenite oxyhydroxysulfate mineral relevant to acid mine drainage. *Am. Mineral.* **92**, 193–197.

Morin G., Ona-Nguema G., Wang Y., Menguy N., Juillot F., Proux O., Guyot F., Calas G. and Brown, Jr., G. E. (2008)

Extended X-ray absorption fine structure analysis of arsenite and arsenate adsorption on maghemite. *Environ. Sci. Technol.* **42**, 2361–2366.

Morin G., Wang Y., Ona-Nguema G., Juillot F., Calas G., Menguy M., Aubry E., Bargar J. R. and Brown, Jr., G. E. (2009) EXAFS and HRTEM evidence for As(III)-containing surface precipitates on nanocrystalline magnetite: implications for As sequestration. *Langmuir* **25**, 9119–9128.

Muehe E. M., Gerhardt S., Schink B. and Kappler A. (2009) Ecophysiology and the energetic benefit of mixotrophic Fe(II) oxidation by various strains of nitrate-reducing bacteria. *FEMS Microbiol. Ecol.* **70**, 335–343.

Ona-Nguema G., Morin G., Juillot F., Calas G. and Brown, Jr., G. E. (2005) EXAFS analysis of arsenite adsorption onto two-line ferrihydrite, hematite, goethite, and lepidocrocite. *Environ. Sci. Technol.* **39**, 9147–9155.

Ona-Nguema G., Morin G., Wang Y., Menguy N., Juillot F. M., Olivi L., Aquilanti G., Abdelmoula M., Ruby C., Bargar J. R., Guyot F., Calas G. and Brown, Jr., G. E. (2009) Arsenite sequestration at the surface of nano-Fe(OH)2, ferrous-carbonate hydroxide, and green-rust after bioreduction of arsenic-sorbed lepidocrocite by *Shewanella putrefaciens*. *Geochim. Cosmochim. Acta* **73**, 1359–1365.

Paktunc D. and Bruggeman K. (2010) Solubility of nanocrystalline scorodite and amorphous ferric arsenate: implications for stabilization of arsenic in mine wastes. *Appl. Geochem.* **25**, 674–683.

Paktunc D., Dutrizac J. and Gertsman V. (2008) Synthesis and phase transformations involving scorodite, ferric arsenate and arsenical ferrihydrite: implications for arsenic mobility. *Geochim. Cosmochim. Acta* **72**, 2649–2672.

Root R. A., Dixit S., Campbell K. M., Jew A. D., Hering J. G. and O'Day P. A. (2007) Arsenic sequestration by sorption processes in high-iron sediments. *Geochim. Cosmochim. Acta* **71**, 5782–5803.

Schwertmann U., Friedl J. and Stanjek H. (1999) From Fe(III) ions to ferrihydrite and then to hematite. *J. Colloid Interf. Sci.* **209**, 215–233.

Sharma P., Ofner J. and Kappler A. (2010) Formation of binary and ternary colloids and dissolved complexes of organic matter, Fe and As. *Environ. Sci. Technol.* **44**, 4479–4485.

Shaw S., Pepper S. E., Bryan N. D. and Livens F. R. (2005) The kinetics and mechanisms of goethite and hematite crystallization under alkaline conditions, and in the presence of phosphate. *Am. Mineral.* **90**, 1852–1860.

Sherman D. M. and Randall S. R. (2003) Surface complexation of arsenic(V) to iron(III) (hydr)oxides: structural mechanism from ab initio molecular geometries and EXAFS spectroscopy. *Geochim. Cosmochim. Acta* **67**, 4223–4230.

Smedley P. L. and Kinniburgh D. G. (2002) A review of the source, behaviour and distribution of arsenic in natural waters. *Appl. Geochem.* **17**, 517–568.

Stookey L. L. (1970) Ferrozine – a new spectrophotometric reagent for iron. *Anal. Chem.* **42**, 779–781.

Sutton N. B., van der Kraan G. M., van Loosdrecht M. C. M., Muyzer G., Bruining J. and Schotting R. J. (2009) Characterization of geochemical constituents and bacterial populations associated with As mobilization in deep and shallow tube wells in Bangladesh. *Water Res.* **43**, 1720–1730.

Sverjensky D. A. and Fukushi K. (2006) A predictive model (ETLM) for As(III) adsorption and surface speciation on oxides consistent with spectroscopic data. *Geochim. Cosmochim. Acta* **70**, 3778–3802.

Szytuła A., Burewicz A., Dimitrijević Ž., Kraśnicki S., Rżany H., Todorović J., Wanic A. and Wolski W. (1968) Neutron diffraction studies of α-FeOOH. *Phys. Status Solidi. B* **26**, 429–434.

Tufano K. J. and Fendorf S. (2008) Confounding impacts of iron reduction on arsenic retention. *Environ. Sci. Technol.* **42**, 4777–4783.

Voegelin A., Kaegi R., Frommer J., Vantelon D. and Hug S. J. (2010) Effect of phosphate, silicate, and Ca on Fe(III)-precipitates formed in aerated Fe(II)- and As(III)-containing water studied by X-ray absorption spectroscopy. *Geochim. Cosmochim. Acta* **74**, 164–186.

Wang Y., Morin G., Ona-Nguema G., Menguy N., Juillot F., Aubry E., Guyot F., Calas G. and Brown, Jr., G. E. (2008) Arsenite sorption at the magnetite-water interface during aqueous precipitation of magnetite. EXAFS evidence of a new surface complex. *Geochim. Cosmochim. Acta* **72**, 2573–2586.

Waychunas G. A., Rea B. A., Fuller C. C. and Davies J. A. (1993) Surface chemistry of ferrihydrite:Part 1.EXAFS studies of the geometry of coprecipitated and adsorbed arsenate. *Geochim. Cosmochim. Acta* **57**, 2251–2269.

WHO (2004) Some drinking-water disinfectants and contaminants, including arsenic. In *IARC Monographs on the Evaluation of Carcinogenic Risks to Human* (ed. WHO). International Agency for Research on Cancer.

Williams A. G. B. and Scherer M. M. (2004) Spectroscopic evidence for Fe(II)–Fe(III) electron transfer at the iron oxide–water interface. *Environ. Sci. Technol.* **38**, 4782–4790.

Zouboulis A. I. and Katsoyiannis I. A. (2005) Recent advances in the bioremediation of arsenic-contaminated groundwaters. *Environ. Int.* **31**, 213–219.

Associate editor: Christopher John Daughney